Desalination and Water Treatment
www.deswater.com
doi: 10.1080/19443994.2013.803795

52 (2014) 4430–4443
June

Taylor & Francis
Taylor & Francis Group

Adsorption of ciprofloxacin on surface functionalized superparamagnetic porous silicas

Parnuch Hongsawat[a,b], Panida Prarat[c], Chawalit Ngamcharussrivichai[d,e], Patiparn Punyapalakul[b,f,*]

[a]*International Postgraduate Programs in Environmental Management, Graduate School, Chulalongkorn University, Bangkok 10330, Thailand*
[b]*Center of Excellence for Environmental and Hazardous Waste Management (EHWM), Bangkok 10330, Thailand*
[c]*Thai Industrial Standards Institute, Ministry of Industry, 75/42 Rama 6 Street, Ratchathewi, Bangkok Thailand*
[d]*Department of Chemical Technology, Faculty of Science, Chulalongkorn University, Bangkok 10330, Thailand*
[e]*Center for Petroleum, Petrochemicals and Advanced Materials, Chulalongkorn University, Bangkok 10330, Thailand*
[f]*Department of Environmental Engineering, Faculty of Engineering, Chulalongkorn University, Bangkok 10330, Thailand*
Tel. +66 2 218 6686; Fax: +66 2 218 6666;

Received 15 August 2012; Accepted 25 April 2013

ABSTRACT

The effect of surface functional groups 3-aminopropyltriethoxy- and 4-(triethoxysilyl)-butyronitrile-, 3-mercaptopropyltriethoxy-, phenyltrimethoxy-, and n-octyl-dimethoxychloro- grafted superparamagnetic particles coated with hexagonal mesoporous silicas (HMS-SPs) on the adsorption of ciprofloxacin (CIP) was evaluated. CIP adsorption followed the pseudo-second-order kinetic model, and intraparticle diffusion was suggested to be the rate-controlling step. Higher CIP adsorption capacities revealed on the hydrophobicity of the adsorbents, however, the phenyltrimethoxy group had the highest adsorption capacity due to the interaction of ¶–¶ electron-donor acceptors. The adsorption capacities strongly depended on an electrostatic interaction, with the exception of the phenytrimethoxy group. The presence of tannic acid (TA) could increase the adsorption capacity of CIP on adsorbent surfaces by multilayer adsorption between a positively charged amine group of CIP and negatively charged TA.

Keywords: Superparamagnetic hexagonal mesoporous silica; Adsorption; Ciprofloxacin; Surface functional group; Tannic acid

1. Introduction

Emerging micropollutants, such as pharmaceutical compounds, hormones, personal care products, and antibiotic compounds, are a major concern in the production of drinking water and the release of wastewater into the environment [1]. Ciprofloxacin (CIP) is a persistent synthetic antibiotic in the fluoroquinolone group that is widely used in infectious symptom treatment. As a consequence of its extensive use in human and veterinary medicine and agriculture, it has been detected in various places such as wastewater, surface

*Corresponding author.

water, production plants, and hospital waste, with a wide range of concentrations (0.2 ppb–60 ppm) [2–5]. Even at low concentrations, CIP could lead to the development of antibiotic-resistant bacteria and has been suggested as an environmental micropollutant hazard. Therefore, the effective removal of CIP has become an increasingly important issue [6].

Various adsorption mechanisms of CIP on carbonaceous adsorbents have been proposed in previous research articles [7,8]. A dispersive interaction has been reported between the free electron of CIP and the delocalized electron in carbon basal planes [7]. Electrostatic attraction and hydrogen bonding via the protonated amine and carboxylic groups of CIP, respectively, seem to play important roles for adsorption on the surface of carbonaceous adsorbents [8]. Similarly to the functionalized silicas, electrostatic interactions and hydrogen bonding were reported in the adsorption interaction at high-concentration levels (ppm) [9]. Cation exchange in soil or clay structures was also reported to be an important interaction for CIP disposition [10,11]. Additionally, a strong interaction between aluminum/iron hydrous oxides and CIP molecules such as the keto- and carboxylate groups was postulated [12]. To the best of our knowledge, uniform organo-functional groups' competitive adsorption of CIP in aqueous solutions at low concentrations (ppb level) has not been studied yet. Moreover, active site competition and/or multilayer adsorption between CIP and coexisting polyphenolic natural organic matter (NOM), such as tannic acid (TA), have been rarely reported in the literature.

Hexagonal mesoporous silicas (HMS), a uniform mesoscale pore and silanol as a surface functional group has been studied extensively in the adsorption and catalysis fields. The surface of HMS can be modified using various methods to enhance specific characteristics (e.g., organic ligand modification) in order to increase selective adsorption capacities. Moreover, superparamagnetic nanoparticles (SP) have been applied as the core of adsorbents to enhance separation efficiencies by adding a magnetic field. For example, the application of superparamagnetic material in classical cake filtration could reduce the overall filtration resistance [13].

The overall goal of this study was to systematically examine and clarify the adsorption mechanisms that controlled CIP adsorption on six types of uniformly functionalized superparamagnetic hexagonal mesoporous silica (HMS-SPs), particularly to understand the roles and effects of hydrophobic interactions, hydrogen bonding, and electrostatic interactions of each organic functional group on CIP adsorption. The physico-chemical characteristics of synthesized HMS-SPs were characterized using various methods. The equilibrium data from the batch experiment were fitted with adsorption isotherm models, and the kinetic parameters were calculated to determine the likely adsorption mechanism. In addition, the effect of the solution pH was investigated. Finally, the effect of TA on CIP adsorption was evaluated and quantitatively analyzed.

2. Materials and methods

2.1. Adsorbent synthesis

2.1.1. Synthesis of superparamagnetic iron oxide particles (SP)

Superparamagnetic iron oxide particles (SP) were synthesized as the core-shell of the adsorbent via coprecipitation from aqueous alkaline solutions modified from the one earlier reported by Qu et al. [14]. In a typical synthesis, $FeCl_3.6H_2O$ (0.046 mol) and $FeSO_4.7H_2O$ (0.023 mol) were dissolved in 150 mL de-ionized water for 3 min. Then, 20 mL ammonium hydroxide (25%) was quickly added into the mixture solution. After 30 min, 3 mL of oleic acid was added into the previous iron solution. The mixture was heated to 75°C and kept at this temperature for 1 h. The SP was collected through magnetic separation and washed with de-ionized water and ethanol three times, then subsequently dried in vacuum conditions.

2.1.2. Synthesis of superparamagnetic hexagonal mesoporous silicas (HMS-SP)

Pristine superparamagnetic hexagonal mesoporous silicas (HMS-SP) was prepared following the procedure described by Tian et al. [15]. A 0.50 g of SP was dispersed in 250 mL of 0.1 M HCl aqueous solution by ultrasonication for 10 min, and this obtained material was separated and washed with deionized water. The as-treated SP was added into the mixture solution of a dodecylaminde (0.35 g), ethanol (3.94 g) and water (27.36 g). The resulting mixture was vigorously stirred at room temperature for 0.5 h. Then, a 2.0 g of tetraethoxysilane (TEOS) was added dropwise to the mixture under vigorous stirring at room temperature for 24 h. After that the material was collected with an external magnetic and washed with deionized water and ethanol to remove nonmagnetic by-products. Subsequently, the obtained powders were extracted by refluxing with ethonal (200 mL) at 80°C for 12 h. This

extraction was repeated for twice to remove the surfactant templates.

2.1.3. Synthesis of organic functionalized HMS-SPs

The organic functionalized HMS-SPs were prepared via postsynthesis using the following procedure: 0.5 g of pristine HMS-SP was dehydrated at 105°C in an oven for 24 h and then stirred in 30 mL of toluene containing 0.5 g of each organosilane: 3-aminopropyltriethoxy-siliane, 4-(triethoxysilyl) butyronitrile, 3-mercaptopropyltriethoxysilane, phenyltrimethoxy-silane, and n-octyldimetholchlorosililane, under refluxing conditions for 24 h to yield A-HMS-SP, N-HMS-SP, M-HMS-SP, P-HMS-SP, and OD-HMS-SP, respectively. The product was filtrated and then washed with 30 mL of toluene. Then, the obtained product was washed with 30 mL of ethanol, except for N-HMS-SP and OD-HMS-SP (OD-HMS-SP and N-HMS-SP were washed with toluene and acetone instead). Finally, the product was dried under a vacuum at 85°C for 2 h.

2.2. Characterization of adsorbents

Surface area, pore volume, and pore size were calculated from nitrogen adsorption isotherms measured at 77 K using an Autosorb-1 Quantachrome automatic volumetric sorption analyzer. Then, the specific surface area, the pore diameter, and the pore volume were all calculated using the Brunauer–Emmett–Teller (BET) theory. Pore size distribution was also calculated using the Barrett–Joyner–Halenda (BJH) equation. The particle diameter was measured by Scanning electron microscopy (SEM JSM 5,800 LV) from ten randomly obtained particles. The presence of organo-functional groups on the synthesized adsorbents' surface was confirmed by a Fourier transform infrared spectrometer (FTIR) (Perkin Elmer Spectrum One). The quantity of nitrogen content on the surface of A-HMS-SP was determined following the procedure described by Smart et al. [16]. A sulfur analyzer (LECO SC132) was used to determine the sulfur content in M-HMS-SP. The hydrophobic/hydrophilic characteristics of the adsorbent surface were evaluated by measuring the water contact angle (θ) using a Dataphysics DCAT-11 tensiometer in a powder contact angle mode. For surface charge determination, 5 mg of adsorbent was suspended in 35 mL phosphate buffer solution with a fixed concentration of 10 mmol L^{-1} and a pH range of 3.0–10.0 for 24 h before the measurement. An electrophoresis apparatus (Zeta-Meter System 3.0, Zeta Meter Inc.) was used to measure the surface charge.

2.3. Adsorbate

CIP was chosen as the representative antibiotic in this study. CIP with a purity of 97% was purchased from Wako pure Co. Ltd. Generally, a CIP molecule consists of a bi-cyclic aromatic ring skeleton with a carboxylic acid group ($pK_{a1} \sim 5.7$–6.1), a ketone group, and a basic-N-moiety ($pK_{a2} = 8.7$). However, the existing CIP species, a cation ($CIPH^+$), zwitterion ($CIP^{\pm}$), and anion (CIP^-), depend on the pH of the solution; therefore, each CIP speciation's persistence was considered and shown in Fig. 1 [17,18].

2.4. Adsorption study

Adsorption isotherm was conducted with an initial CIP and TA concentration range between 10–300 μg L^{-1} and 1–200 mg L^{-1}, respectively. Concentration of adsorbents was kept at 1 g L^{-1}. The ionic strength of the solution was fixed at 0.01 M using phosphate buffer at either pH 5, 7 or 9. The sample was shaken at 220 rpm at 25°C, and then, the supernatant solution was filtrated through a glass filter (GF/C, pore size 0.45 mm). The adsorption kinetics was studied by varying the equilibrium contact time from 0 to 180 min. The initial concentration of CIP was 250 μg L^{-1}. The pH and ionic strength of the solution were fixed at pH 7 and 0.01 M, respectively. The filtrated solute underwent a solid-phase extraction (SPE) with PEP cartridges (200 mg/6 mL, Cleanert PEP-H). The cartridges were equilibrated with methanol (5 mL) and water (10 mL), and then, the filtrate sample was taken, eluted with methanol (10 mL), evaporated and then resuspended with 0.5 mL of methanol. The quantities of CIP concentration in equilibrium solutions were analyzed by a reverse phase high-performance liquid chromatography (HPLC) equipped with a photodiode array detector (280 nm). The determination of CIP in the solution was performed at 50°C on a HPLC column (5 mm, 250 mm × 4.6 mm; LiChrosorb NH_2, GLS Sciences, USA). The elution gradient was conducted using acetonitrile (A) and water (B). The initial elution condition was a mobile phase A 100% v/v reach to 0% v/v within 15 min. The flow rate was 1 mL min^{-1}. Sulfamethoxazole was spiked in the obtained sample solution as the surrogate standard. Then, the adsorption capacity was calculated from the difference between initial and equilibrium concentration divided by the amount of adsorbent.

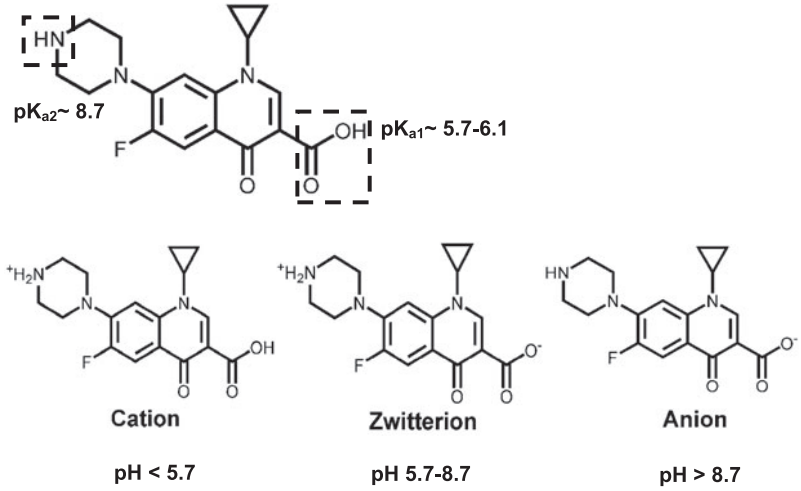

Fig. 1. Molecular structure of CIP speciation at different pH.

2.5. Effect of tannic acid on CIP adsorption

TA was selected as a representative of NOM with a molecular weight of approximately 1,700 Da. The effect of TA on CIP adsorption was investigated by adjusting the TA solution (40 mg/L) to different CIP concentration at pH 7.0 and 0.01 M of phosphate buffer. The residual concentration of TA in the solution was analyzed by the HPLC equipped with a photodiode array detector (280 nm). The separation was performed at 50°C on a C18 HPLC column (5 mm, 250 × 4.6 mm; Intersil, GLS Sciences, USA) using an acetronitrile-water mixture (85:15%, v/v) as the mobile phase at a flow rate of 1 mL min^{-1}. The quantities of CIP in the presence of TA were analyzed via the same adsorption procedure. The presence of TA interfered with the recovery of CIP; therefore, double PEP cartridges (200 mg/6 mL, Cleanert PEP-H) were used in the same SPE procedure to increase the recovery efficiencies.

3. Results and discussion

3.1. Physical characteristics of adsorbents

Surface area, pore size, and pore volume of HMS-SP and functionalized HMS-SPs were calculated from nitrogen adsorption isotherm data and are summarized in Table 1 (the nitrogen adsorption–desorption isotherm data were shown in Fig. S1 in the Supplementary data). According to the obtained results, since the size of CIP molecular dimension was smaller than the pore size of all the adsorbents [10], the CIP molecules could be available for adsorption both on the external and internal surface areas of the synthesized adsorbents. Moreover, due to the higher molecular size of TA (2.7 and 2.8 nm in width and length, respectively) than CIP molecule, it can be deduced that CIP should be more accessible to the inner pores than TA.

The contact angle of each adsorbent was obtained in the following order: OD-HMS-SP > P-HMS-SP > M-HMS-SP >> N-HMS-SP ~ A-HMS-SP > HMS-SP (Table 1). Based on the contact angle value, the synthesized adsorbents can be classified into two categories: hydrophobic adsorbent surfaces (OD-HMS-SP, P-HMS-SP, and M-HMS-SP) and hydrophilic adsorbent surface (N-HMS-SP, A-HMS-SP, and HMS-SP).

Fig. 2 shows the surface charge density of pristine HMS-SP and functionalized HMS-SPs as the function of pH. The pH at a zero point charge (pH$_{zpc}$) of pristine HMS-SP was 4.5. Most of the functionalized HMS-SPs exhibited a shift up from HMS-SP except OD-HMS-SP (Table 1). Thus, most of the organo-functional groups on adsorbent surface undergo protonation at moderate or low-pH values. To the contrary, the amine functional group of A-HMS-SP was protonated until the pH 9.0.

The presence of 3-aminopropyltriethoxy and 3-mercaptopropyltriethoxy functional groups can be investigated by determining the nitrogen and sulfur content on their surfaces. The amine group content of A-HMS-SP was 39.28 $\mu mol_N\, m^{-2}$ and the sulfur content of M-HMS-SP was 1.94 $\mu mol_s\, m^{-2}$, confirming the presence of 3-aminopropyltriethoxy and 3-mercaptopropyltriethoxy functional groups on the surfaces of A-HMS-SP and M-HMS-SP, respectively (Table 1).

Table 1
Physical and chemical characteristics of adsorbents

Adsorbents	Surface functional groups	Surface characteristics[a]	Contact angle (θ)	Pore diameter (nm)	BET surface area (m^2/g)	Pore volume (mm^3/g)	Particle diameter (μm)	pH_{zpc}
SP	–	–	–	–	95	–	0.14	–
HMS-SP	Silanol	Hydrophilic	45	3.28	380	344	0.33	4.5
A-HMS-SP	Amino	Hydrophilic	50	3.70	141	265	0.15	9.0
N-HMS-SP	Nitrile	Hydrophilic	53	3.32	362	589	0.21	4.5
M-HMS-SP	Mercapto	Hydrophobic	60	2.51	492	609	0.39	6.4
P-HMS-SP	Phenyl	Hydrophobic	77	2.52	345	471	0.21	5.5
OD-HMS-SP	Octyl	Hydrophobic	90	3.21	403	237	0.18	3.5
PAC[b]	Carboxyl, phenyl and oxygen-containing group	Hydrophobic	58	1.90	980	–	–	9.5

[a]Contact angle was used to identify the hydrophilic/hydrophobic surface characteristics of adsorbent.
[b]Refs. [20,32].

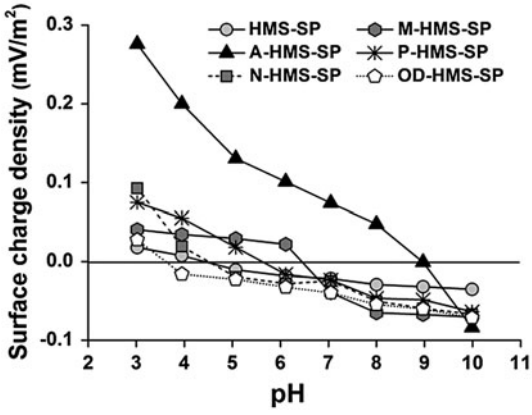

Fig. 2. Surface charge density of synthesized HMS-SP and functionalized HMS-SPs as a function of the solution pH at ionic strength (IS) 0.01 M.

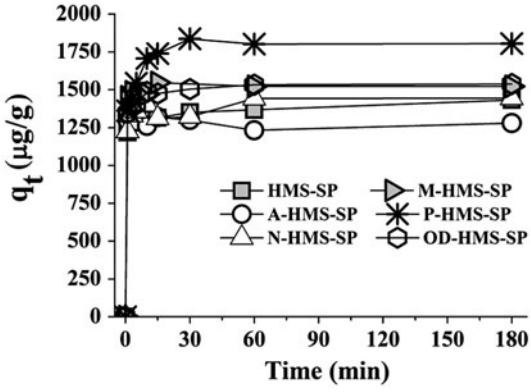

Fig. 3. Adsorption kinetics of CIP by HMS-SP and functionalized HMS-SPs.

3.2. Adsorption kinetics

The CIP adsorption kinetics were evaluated and expressed in Fig. 3. The CIP uptake by all synthesized adsorbents increased gradually in the first 15 min, and then, the equilibrium stage was reached after approximately 30 min. Both pseudo-first-order and pseudo-second-order adsorption kinetics models were determined; however, the experimental data were well-fitted with the pseudo-second-order kinetic model (Table 2). The pseudo-second-order can be expressed as follows:

$$\frac{t}{q_t} = \frac{1}{k_2 q_e^2} + \frac{t}{q_e} \quad (1)$$

where k_2 is the rate constant for pseudo-second-order, and q_t and q_e are the amount of CIP adsorbed at any given time t (min) and at equilibrium ($\mu g\, g^{-1}$), respectively. For the same initial concentration of kinetic studies, the adsorption capacities of the hydrophobic adsorbents (M-HMS-SP, P-HMS-SP, and OD-HMS-SP) were higher than the hydrophilic adsorbents (HMS-SP, A-HMS-SP, and N-HMS-SP). On the other hand, the initial adsorption rate (h) increases in the order of N-HMS-SP < HMS-SP < P-HMS-SP ~ OD-HMS-SP < A-HMS-SP ~ M-HMS-SP as shown in Table 2. A higher initial adsorption rate of A-HMS-SP and M-HMS-SP was observed than the other synthesized adsorbents. These results suggest that not only is the hydrophobic interaction involved in CIP adsorption, but other interactions may also be involved, such as hydrogen bonding and electrostatic attractive forces. However, the initial adsorption rate and the adsorption capacity of all synthesized HMS-SPs were both still lower than conventional powdered activated carbon (PAC) due to

Table 2
Kinetic parameters of CIP adsorption on HMS-SP and functionalized HMS-SPs (at pH 7 and IS of 0.01 M)

Adsorbents	$q_{e.exp}$ (μg g^{-1})	Pseudo-second-order				
		$q_{e,cal}$ (μg g^{-1})	k_2 (g μg^{-1} min^{-1})	R^2	h [a] (μg g^{-1} min^{-1})	$t_{0.5}$ [b] (min)
Hydrophilicity						
HMS-SP	1,367	1,429	0.001	0.9997	2,042	0.70
A-HMS-SP	1,318	1,250	0.013	0.9998	20,313	0.06
N-HMS-SP	1,442	1,423	0.001	0.9997	2,025	0.70
Hydrophobicity						
M-HMS-SP	1,547	1,429	0.010	0.9999	20,420	0.07
P-HMS-SP	1,802	1,667	0.002	0.9998	5,558	0.30
OD-HMS-SP	1,533	1,667	0.002	0.9999	5,558	0.30
PAC	2,213	5,000	0.0002	0.9999	33,333	1.00

[a]h = initial adsorption rate (μg g^{-1} min^{-1}) calculated from $h = k_2 q_e^2$.
[b]$t_{0.5}$ = half life of CIP adsorption calculated from $t_{0.5} = 1/k_2 q_e$.

complexation of organo-functional group on its surface (the kinetic results of PAC are shown in Table S2 in the supplementary data).

As the pseudo-second-order kinetics model was not able to identify the deep diffusion mechanism of the porous material, an intraparticle diffusion model based on the theory proposed by Weber and Morris was applied [19–21]. The governing equation can be written as:

$$q_t = k_{1P_i} \cdot t^{0.5} + C_i \quad (2)$$

where q_t, k_{1P_i}, and C_i are the amount adsorbed at time t (μg g^{-1}), the intraparticle rate constant of stage i (μg g^{-1} $h^{-0.5}$), and the intercept of stage i, respectively.

The multilinearized plot of q_t vs. $t^{0.5}$ based on the intraparticle diffusion model of CIP was observed on all synthesized adsorbents as shown in Fig. 4. The slope-fitting plots did not pass through the origin for all adsorbents. It implies that not only the intraparticle diffusion in the adsorption mechanism, but also the film diffusion affects CIP adsorption [21]. The rate parameters of CIP with each of the synthesized adsorbent are listed in Table 3. In the adsorption process, the rate is controlled by the slowest stage. The synthesized adsorbents (except P-HMS-SP) exhibited two different diffusion stages, indicating that the rate was governed by intraparticle diffusion (k_{1P_1}) and film diffusion might be quite rapid, hence it could not be observed. On the other hand, the plot of P-HMS-SP consists of three linear portions; therefore, CIP adsorption was controlled more by the lower rate intraparticle diffusion (k_{1P_2}) than film diffusion (k_{1P_1}).

For film diffusion, the intercept C of intraparticle diffusion can indicate a film layer effect. A larger film layer thickness was achieved using the greater intercept C. As shown in Table 3, OD-HMS-SP has the lowest C value, indicating that it has the lowest film diffusion effect consistent with the hydrophobic surface level where the water film resistance surrounding the adsorbent particle might be reduced. Hence, CIP can be transported more easily from the liquid film layer to the external surface of hydrophobic OD-HMS-SP than the other lower hydrophobic adsorbents.

In order to determine the actual rate-controlling step in the CIP adsorption; the kinetic data were analyzed using the procedure of Malash et al. [22] expressed as:

$$F(t) = \frac{q}{q_e} \quad (3)$$

for $F(t)$ values > 0.85

$$Bt = 0.4977 - \ln(1 - F(t)) \quad (4)$$

for $F(t)$ values < 0.85

$$Bt = \left(\sqrt{¶} - \sqrt{¶ - (¶^2 F(t)/3)}\right)^2 \quad (5)$$

where $F(t)$ is the fractional attainment of equilibrium at different times t, ¶ is the constant (approximately 3.1416) and B_t is a function of $F(t)$. By plotting B_t against time, the rate-controlling step can be distinguished (data were shown in Fig. S2 in the supplementary data). The CIP adsorption data were more scattered and did not pass through the origin, which might indicate film diffusion [23,24]. However, these results are still not sufficient to clarify the rate-controlling step. Thus, the film diffusion coefficient

(D_1) and the pore diffusion coefficient (D_2) are determined using the following equation [19]:

$$\frac{q_1}{q_e} = 6\left(\frac{D_1}{\P r^2}\right)^{0.5} t^{0.5} \quad (6)$$

$$B = \P^2 \frac{D^2}{r^2} \quad (7)$$

In this equation, r represents the radius of the particle, assuming spherical particles. The film diffusion coefficient (D_1) value is calculated from the slope of the plots of q_t/q_e vs. t. The pore diffusion coefficient (D_2) value is calculated from the slope (B) of the plot of B_t vs. t.

The film diffusion coefficient (D_1) and the pore diffusion coefficient (D_2) are shown in Table 3. The pore diffusion coefficient (D_2) is lower than the film diffusion coefficient (D_1) with all synthesized adsorbents. These indicate that the rate-controlling step for CIP adsorption is governed by intraparticle diffusion. According to the D_2 values of hydrophilic adsorbents (HMS-SP, A-HMS-SP, and N-HMS-SP), the N-HMS-SP had a ~2.25-fold lower pore diffusion rate (D_2) than HMS-SP and ~1.88-fold lower than A-HMS-SP even though the mean pore size of N-HMS-SP was not significantly different. The wider pore size distribution of N-HMS-SP (data were shown in Fig. S1 in the supplementary data) was likely to affect the CIP diffusion process into the mesopores, which resulted in a lower pore diffusion rate. In addition, the D_2 values of the hydrophobic adsorbents (M-HMS-SP and P-HMS-SP), with the exception of OD-HMS-SP, were lower than the hydrophilic adsorbents, in accordance with their significantly smaller mean pore sizes (Table 1).

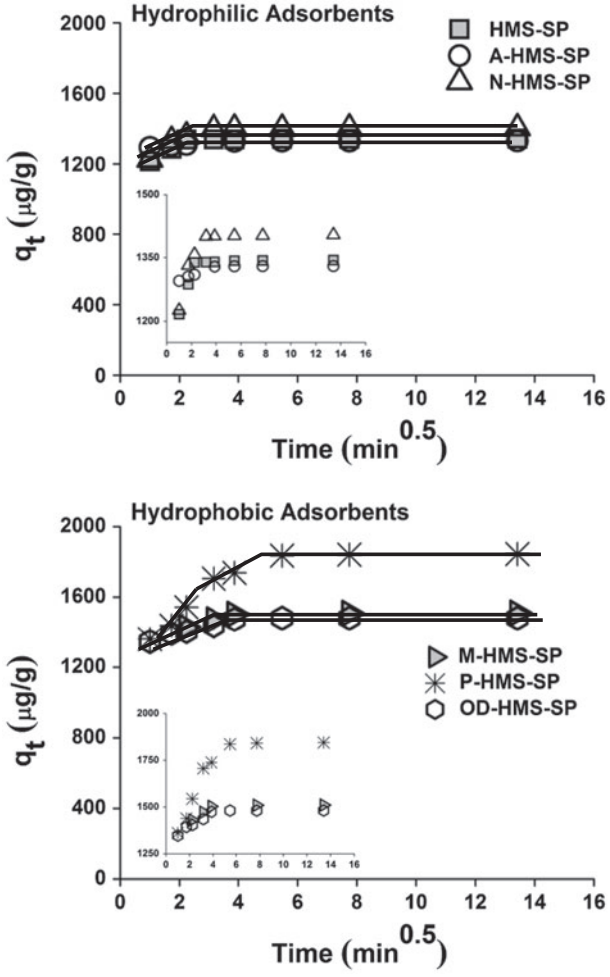

Fig. 4. Intraparticle diffusion model fitting of the CIP adsorption kinetics on synthesized adsorbents.

3.3. Adsorption isotherms

3.3.1. Adsorption mechanism

The adsorption isotherm of CIP on each adsorbent at pH 7.0 is shown in Fig. 5(a). The results revealed that the hydrophobic adsorbents (P-HMS-SP > OD-HMS-SP ~ M-HMS-SP) have higher CIP adsorption capacities than hydrophilic adsorbents (N-HMS-SP > HMS-SP > A-HMS-SP). Among hydrophobic adsorbents, P-HMS-SP has the highest adsorption capacity without relying on the order of the contact angle value (OD-HMS-SP > P-HMS-SP > M-HMS-SP) (Table 1). This might be a result of the dispersive interaction between the ¶ electrons in the aromatic ring of CIP and the phenyl group on its surface or the interaction between the ¶ electrons in the phenyl group and the free electrons in CIP molecules (7). The adsorption of CIP on OD-HMS-SP displayed a comparable adsorption capacity to M-HMS-SP, although OD-HMS-SP has a higher hydrophobic surface as reflected by the contact angle value (Table 1), which suggests a combination between the hydrophobic force and hydrogen bonding via mercapto functional groups of M-HMS-SP. For hydrophilic adsorbents, hydrogen bonding between active functional groups of CIP molecules (such as carboxylic-, ketone-, fluoride-, and basic N-group) and surface functional groups with –OH, $–NH_2$, or –CN moieties of HMS-SP, A-HMS-SP, and N-HMS-SP, respectively, was assumed to involve in the adsorption mechanism.

In order to neglect the effect of the adsorbents' surface areas, the adsorption capacities were standardized for surface area differences in terms of surface density as μg m^{-2} as shown in Fig. 5(b). The CIP

Table 3
Intraparticle diffusion parameters (Weber and Morris model) and diffusion coefficients (Boyd model) for the adsorption of CIP on adsorbents (at pH 7 and IS of 0.01 M)

Adsorbents	Intraparticle diffusion						Film diffusion[c]	Pore diffusion[d]
	k_{1P_1}[a] ($\mu g\,g^{-1}\,min^{-1/2}$)	C_1	R^2	k_{1P_2}[b] ($\mu g\,g^{-1}\,min^{-1/2}$)	C_2	R^2	$D_1 \times 10^{-4}$ ($\mu m^2\,min^{-1}$)	$D_2 \times 10^{-4}$ ($\mu m^2\,min^{-1}$)
Hydrophilicity								
HMS-SP	99	1,118	0.99	–	–	–	19.5	1.8
A-HMS-SP	8	1,290	0.94	–	–	–	5.6	1.5
N-HMS-SP	78	1,177	0.90	–	–	–	7.0	0.8
Hydrophobicity								
M-HMS-SP	70	1,266	0.95	–	–	–	30.2	0.3
P-HMS-SP	163	1,181	0.99	57	1,522	0.99	7.3	1.1
OD-HMS-SP	62	848	0.96	–	–	–	3.7	1.8

[a]Calculated at the first stage of the diffusion. [b]Calculated at the second stage of the diffusion. [c]Calculated from Eq. (6). [d]Calculated from Eq. (7).

adsorption density of the hydrophobic adsorbents was in the order of P-HMS-SP ~ OD-HMS-SP > M-HMS-SP and was higher than those of the hydrophilic adsorbents. This indicated that the hydrophobic interaction (i.e., van der Waals force) was likely to be the major CIP adsorption mechanism. Nevertheless, it can be seen that A-HMS-SP provided a comparable adsorption capacity per square meter to the hydrophobic adsorbents. This might be caused by a combination of an attractive electrostatic interaction and hydrogen bonding. At pH 7, the A-HMS-SP had a more positively charged surface compared with other synthesized adsorbents; thus a negative part of CIP zwitterionic molecules might be electrostatically attracted to the positive charged surface via electrostatic interaction.

In order to investigate the electrostatic interaction's effect on the adsorption mechanism, CIP on pristine HMS-SP and functionalized HMS-SPs was investigated by varying the pH at pH 5, pH 7, and pH 9. In Fig. 6, the CIP adsorption capacities on HMS-SP, N-HMS-SP, M-HMS-SP, and OD-HMS-SP were significantly affected by the pH, which strongly confirmed the supposed mechanism of the electrostatic interaction as discussed above. In contrast, it is possible that the electrostatic interaction might not be involved in CIP adsorption for P-HMS-SP, which had the highest adsorption capacities. The interaction of ¶–¶ electron-donor acceptors of the phenyl-functional group on the P-HMS-SP surface might be the key role in the adsorption mechanism. Moreover, the electrostatic interaction did not seem to be the dominant adsorption mechanism on A-HMS. As seen in Fig. 6, the adsorption capacity of CIP onto A-HMS-SP at pH 7 was higher than at pH 5 and 9. One possible explanation is that CIP adsorption might be enhanced due to the combination of the electrostatic interaction between the positively charged amine group and the negative part of the CIP zwitterionic molecule, and the hydrogen bonding between the amine group and/or residual silanol group (nongrafted silanol) and the active carboxylic-, ketone-, fluoride-, and basic nitrogen-groups of CIP molecules, leading to a higher adsorption capacity.

According to the low equilibrium concentration range (0–20 $\mu g\,L^{-1}$), the CIP adsorption capacities were investigated by varying the pH at 5, 7, and 9, and the results were illustrated in the inset of Fig. 6. It was observed that the adsorption trends on HMS-SP, M-HMS-SP, and OD-HMS-SP were as the same as those at high concentrations, suggesting that the presence of water molecules did not significantly affect the CIP adsorption mechanism of those three adsorbents. In addition, A-HMS-SP, N-HMS-SP, and P-HMS-SP displayed higher CIP adsorption capacities at pH 5 and 9 than at pH 7. This implies that it might be caused by the effect of hydronium and/or hydroxide ions in aqueous phase competed and/or balanced the active sites of adsorbent surface or adsorbate.

For the CIP adsorption on PAC, it showed quite higher adsorption capacity than the synthesized adsorbent that might be caused by its complexity of surface functional groups and higher surface area (Fig. 5(a) and Fig. 6). However, the CIP adsorption capacities per surface area of the entire synthesized

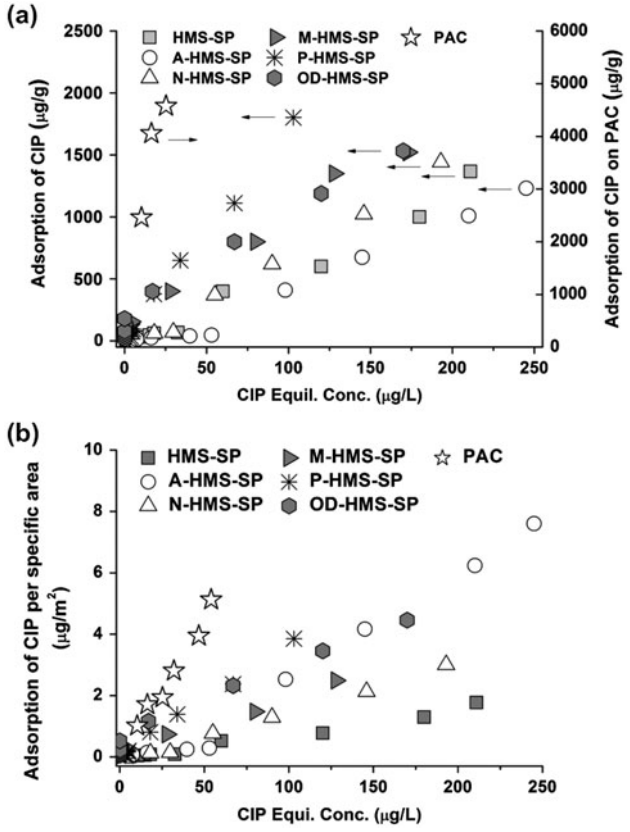

Fig. 5. Effect of organo-functional groups on the adsorbent surface onto (a) adsorption capacities of CIP (b) adsorption capacities of CIP per specific surface area in 0.01 M phosphate buffer pH 7.

adsorbents were slightly lower than PAC which indicated that the high affinity of organo functional groups could enhance the CIP adsorption capacities (Fig. 5(b)). Thus, these results are the useful information leading to the development of synthesized adsorbent with high-adsorption affinity, high selectivity, and high surface area that can enhance the CIP adsorption efficiency.

3.3.2. Isotherm models

According to the adsorption isotherm at concentration ranges (100–10,000 μg L^{-1}), the traditional approaches of determining the isotherm parameters, Langmuir and Freundlich isotherm models, were used to test the experimentally derived adsorption process data for correlation. However, the adsorption isotherms at a low equilibrium concentration range (up to 20 μg L^{-1}) were investigated via the linear adsorption isotherm model. The Langmuir (8), Freundlich (9), and linear (10) adsorption isotherm models can be expressed as:

$$q_e = q_m K_L C_e/(1 + K_L C_e) \quad (8)$$

$$q_e = K_F C_e^{\frac{1}{n}} \quad (9)$$

$$q_e = K_p C_e + C \quad (10)$$

where K_L is the adsorption equilibrium constant, q_m is the maximum adsorption capacity (μg g^{-1}), and C_e is the equilibrium concentration (μg L^{-1}). K_F and n are Freundlich constants, K_p, and C indicate the linear partition coefficient and the interception obtained from the slope of plotted q_e vs. C_e, respectively. A higher K_F or K_p value indicates a higher affinity between CIP and the adsorbent.

The obtained isotherm parameters with a high range of CIP concentrations were estimated by Origin Pro version 8.5, which revealed no relationship with the Langmuir isotherm, but the data were well-fitted with the Freundlich isotherm, as shown in Table 4. Hydrophobic adsorbents have higher K_F values than hydrophilic adsorbents in every pH (pH 5–9). However, pristine HMS-SP shows a higher affinity with CIP at pH 5 and pH 7 compared with hydrophobic ones. These results suggested that CIP adsorption might have a high affinity with attractive electrostatic interactions, which might be supported by hydrogen bonding with a silanol group. However, this adsorption behavior is further discussed as it relates to the adsorption mechanism.

As shown in the insert of Fig. 6, the adsorption of CIP at low equilibrium concentrations was best fitted to the linear-shaped adsorption isotherm to all adsorbents with a high correlation coefficient ($R^2 > 0.93$). While the linear-adsorption isotherm parameter was shown in Table 4, two adsorption behaviors were obtained for CIP adsorption on the synthesized adsorbents. The first is the immediate adsorption at very low initial concentrations which was implied from the positive intercept C (hydrophobic adsorbents). The second behavior was the negative intercept C that can be used to assume that CIP is not adsorbed on the adsorbent at very low concentrations (hydrophilic adsorbents).

3.4. Adsorption of tannic acid

Concerning the fate and transport of antibiotics in the environment, the effect of NOM on the adsorption of antibiotics has been investigated in several reports [25,26]. TA, consisting of hydrophilic phenolic groups and hydrophobic aromatic rings, was selected to be the model of NOM in this study. The adsorption isotherms of TA at pH 7.0 onto the six synthesized

Table 4
Isotherm parameter of the Freundlich and Linear model for the CIP adsorption onto adsorbents (at pH 7 and IS of 0.01 M)

Adsorbents	pH	Freundlich isotherm*			Linear adsorption isotherm**		
		K_F (μg/g)	$1/n$	R^2	Kp (μg/g)	C	R^2
HMS-SP	5	76	0.69	0.98	23	18	0.96
	7	46	0.56	0.90	6	−56	0.98
	9	1	0.88	0.97	9	−84	0.97
A-HMS-SP	5	4	0.86	0.98	45	−139	0.99
	7	8	0.86	0.96	5	−97	0.98
	9	27	0.45	0.98	41	−21	0.93
N-HMS-SP	5	22	0.91	0.99	62	−21	0.98
	7	6	0.18	0.93	8	−63	0.99
	9	86	0.39	0.98	91	−8	0.93
M-HMS-SP	5	17	1.06	0.99	53	3	0.98
	7	30	0.79	0.97	9	75	0.99
	9	9	0.86	0.99	11	18	0.91
P-HMS-SP	5	114	0.58	0.99	37	32	0.90
	7	41	0.82	0.99	17	−2	0.99
	9	24	0.87	0.99	108	−193	0.98
OD-HMS-SP	5	36	0.83	0.98	18	56	0.90
	7	182	0.42	0.99	9	113	0.98
	9	58	0.47	0.95	56	−127	0.99

*Obtained result within the high concentration range (0–600 μg/L).
**Obtained result within the low concentration range (0–20 μg/L).

adsorbents were shown in Fig. 7. A-HMS-SP had the highest adsorption capacity of TA comparing with all the synthesized adsorbents. This is in consistence with the notion of previous reports that the positively charged surface of amine groups could enhance the adsorption capacity of TA and the electrostatic interaction was suggested to be the main adsorption mechanism [13,27,28].

3.5. Effect of tannic acid on CIP adsorption

As revealed in Fig. 7, A-HMS-SP and OD-HMS-SP had the highest and lowest TA adsorption capacities, respectively. Therefore, hydrophilic A-HMS-SP and hydrophobic OD-HMS-SP were chosen to study the effect of TA on CIP adsorption.

Fig. 8 shows the adsorption of CIP by A-HMS-SP and OD-HMS-SP at pH 7.0 and IS 0.01 M in coexisting solution with and without TA. The findings were consistent with previous results that A-HMS-SP and OD-HMS-SP were preferable for TA and CIP adsorption, respectively. However, the adsorption capacity of CIP on A-HMS-SP in mixed solute was extremely increased in the presence of TA, while the adsorption capacity of TA on A-HMS-SP was not significantly affected. TA might form a layer on the surface via the interaction between the TA molecules and the amine groups on its surface due to the electrostatic interaction between the negatively charged TA molecules and the positively charged amine functional groups on the surface of A-HMS-SP [13,27,28]. Then, CIP ($CIP^{\pm}$) molecules can create a new layer on the former layer of TA via the formation between protonated amine groups of CIP molecules and deprotonate carboxylic groups of TA molecules ($pKa \approx 5.7$), which might increase the CIP adsorption capacity on A-HMS-SP via an electrostatic interaction. In common with recent reports, the electrostatic interaction between the specific ligand of folic acid and the amino-propyl functionalized mesoporous silica surface or the amine groups on the surface of the silica played a key role in adsorption mechanism [29]. Additionally, the negative surface charge of the condensed cationic Na^+ interacted with a polyamidoamine (amine functional group) dendrimer during the zeolite formation process via an electrostatic interaction [30].

In the case of OD-HMS-SP, there was a slightly increased CIP adsorption capacity in the presence of TA. This might be due to the formation of TA and CIP ($CIP^{\pm}$) molecules via an electrostatic attraction

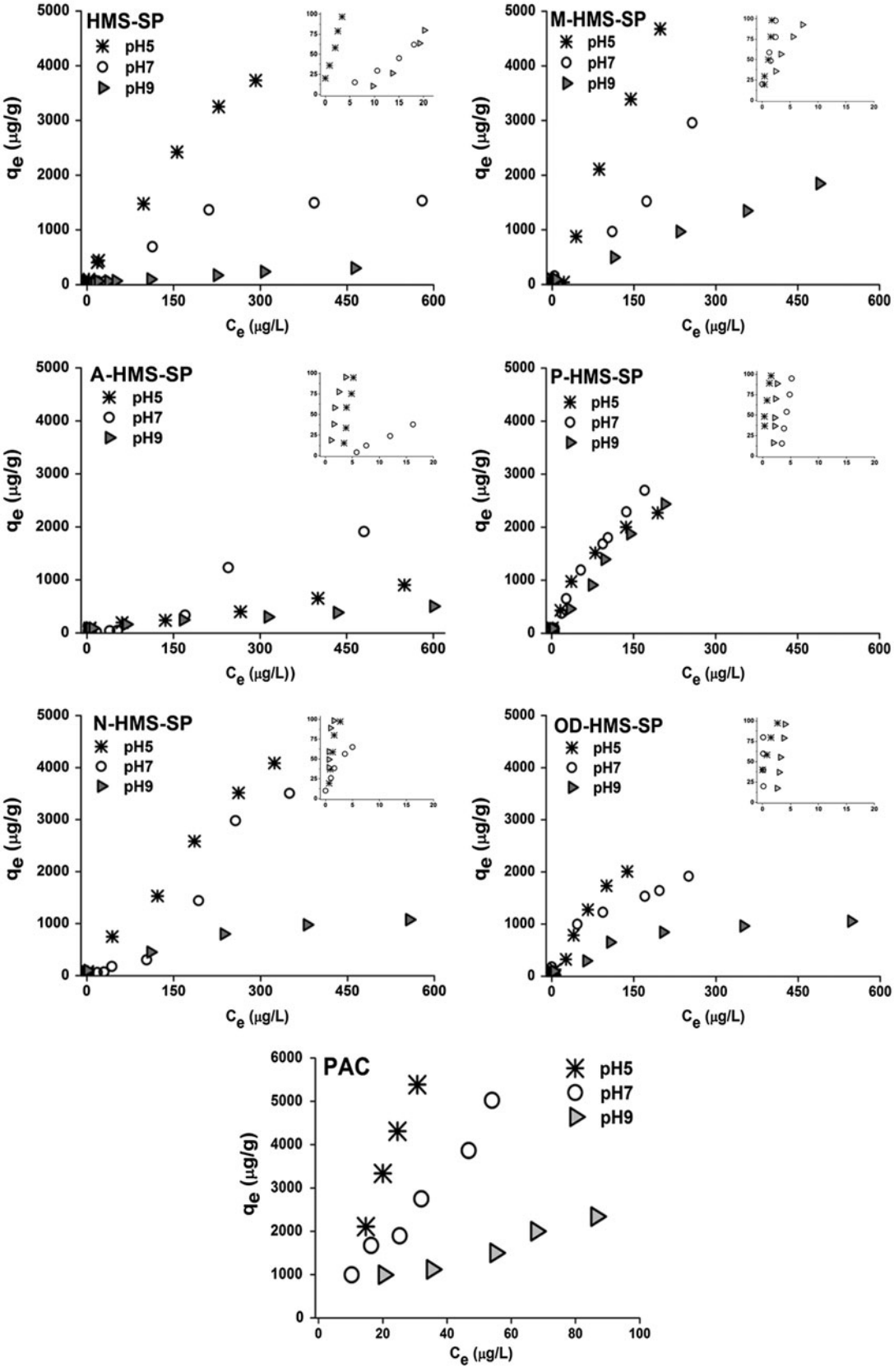

Fig. 6. Adsorption isotherm of CIP onto HMS-SP, functionalized HMS-SPs and PAC in 0.01 M phosphate buffer pH 5, pH 7, and pH 9.

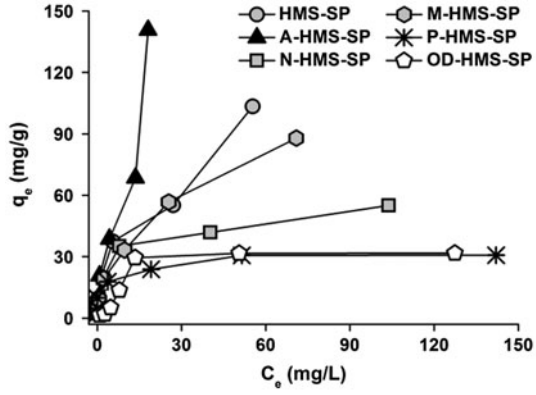

Fig. 7. Adsorption isotherm of Tannic acid onto HMS-SP and functionalized HMS-SPs in 0.01 M phosphate buffer pH 7.

similar to that of A-HMS-SP in the second layer. Furthermore, the adsorption capacity of TA increased slightly compared with a single solute. This phenomenon can be explained by the multilayer adsorption between TA and CIP associated with an interaction between TA and CIP via amine function groups of CIP without the specific selectivity of *n*-octyldimethoxy surface. Further studies could utilize these obtained adsorption mechanism for predicting the fate and transportation of antibiotic compounds.

Moreover, according to a previous report, the organo-functional groups on the surface of mesoporous silica can interact among them as an organic network based on hydrogen bond interaction. As a result, the pore system is not completely accessible to small compounds. Acid washing can labilize hydrogen bonds and open the network to increase the internal surface accessibility of target compounds [31]. Further studies could use acid washing to elucidate the antibiotic adsorption interaction in greater detail.

3.6. Comparative assessment of various adsorbents and environmental implication

Adsorption capacities per surface area of CIP onto the various adsorbents by different investigators from aqueous solution at the same equilibrium concentration of 250 μg L^{-1} are compared and shown in Table 5. Notably, the Freundlich-based adsorption capacity (q_e) was applied due to the best fit in this study, whereas the q_e of other adsorbents reported in the literature derived from the Langmuir-based. The CIP adsorption capacities of all synthesized adsorbents seem to be lower than the other adsorbents. However, the equilibrium adsorption time for all synthesized adsorbents found in our studies is quite fast (0.5 h), whereas most

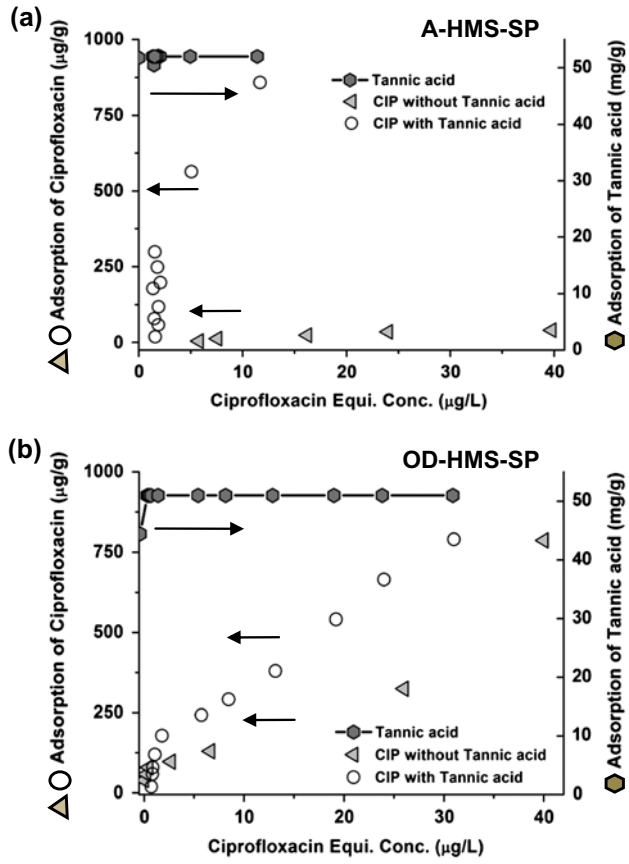

Fig. 8. Effect of tannic acid on the adsorption of CIP onto (a) A-HMS-SP, and (b) OD-HMS-SP in 0.01 M phosphate buffer pH 7.

of the other adsorbents exhibited the very slow adsorption kinetics (such as activated carbon~3 d, carbon xerogel~3 d, carbon nanotubes~3 d, aluminum and iron hydrous oxide~1 d, goethite~6 h, kaolinite~8 h, modified coal fly ash~2 h, montmorillonite~7–24 h for CIP adsorption).

Even the PAC seems to have great potential as adsorbent for CIP removal due to high adsorption capacities and fast equilibrium time, the high selectivity caused by grafted surface functional groups is found in our study. Moreover, the synthesized adsorbents can be easily separated from aqueous solution due to the superparamagnetic property by installing a magnetic field in the adsorption process. With this respect, the combination between filtration and magnetic separation is applied into the industrial scale such as the high gradient magnetic separation. Furthermore, the cake filtration could reduce the overall filtration resistance in the superparamagnetic system [13,36].

Table 5
Comparative assessment of CIP adsorption on different adsorbents

Adsorbents	C_i (mgL^{-1})	Temp (°C)	pH	q_e[a] (μgm^{-2})	t_{equi}[b] (h)	Reference
HMS-SP	0.1–10	25	7.0	3	0.5	Present study
A-HMS-SP	0.1–10	25	7.0	7	0.5	Present study
N-HMS-SP	0.1–10	25	7.0	0.04	0.5	Present study
M-HMS-SP	0.1–10	25	7.0	5	0.5	Present study
P-HMS-SP	0.1–10	25	7.0	11	0.5	Present study
OD-HMS-SP	0.1–10	25	7.0	5	0.5	Present study
PAC	0.1–10	25	7.0	22	0.5	Present study
Activated carbon (AC)	3–30	25	5.0	72	Three day	[7]
Carbon xerogel (CX)	3–30	25	5.0	32	Three day	[7]
Carbon nanotubes (CNT)	3–30	25	5.0	82	Three day	[7]
Aluminum hydrous oxide (HAO)	0.2–165	25	7.1	35	24	[12]
Iron hydrous oxide (HFO)	0.2–165	25	7.1	68	24	[12]
Geothite	0.33–331	22	5.0	18	6	[33]
Kaolinite	33–663	RT[c]	3.0–4.5	196	8	[10]
Modified coal fly ash (MCFA)	40–140	25	Not adjusted	58	2	[34]
Montmorillonite (MMT)	500–4,000	RT[c]	5.0	231	24	[11]
	500–2,500	37	3.0	386	7	[17]
		37	11.0	7	7	[17]
Montmorillonite (SAz-1)	500–4,000	RT[c]	4.0–5.5	524	0.25	[35]
Rectorite	150–2,000	RT[c]	4.0–5.5	358	0.25	[35]

[a]q_e = adsorption capacity at equilibrium concentration of 250 μgL^{-1} (mgg^{-1}) (calculated by the best suitable isotherm).
[b]t_{equi} = time at equilibrium (h).
[c]RT = room temperature or ambient condition.

4. Conclusion

The CIP adsorption mechanism on HMS-SP and functionalized HMS-SPs was well fitted to the pseudo-second-order kinetics model. The rate-controlling step in the adsorption interaction appeared to be intraparticle diffusion. Hydrophobic adsorbents had higher adsorption capacities than hydrophilic adsorbents. The phenyltrimethoxy group had the highest adsorption capacity due to the interaction of ¶–¶ electron-donor acceptors. The adsorption capacities strongly depended on electrostatic interactions (with the exception of the phenyltrimethoxy-group). However, when CIP has a low equilibrium concentration (0–20 ppb), the hydronium and/or hydroxide ions of water might affect the CIP adsorption capacities of some surface functional groups. Furthermore, the presence of TA, representing NOM, could increase the adsorption capacities of CIP on adsorbent surfaces by multilayer adsorption via an electrostatic interaction between the protonated amine group of CIP and negatively charged TA.

Acknowledgments

The authors are grateful for the financial support from the 90th Anniversary of Chulalongkorn University Fund (Ratchadaphiseksomphot Endowment Fund). This work is conducted under the research cluster "Control of Emerging Micropollutants in Aquacultural and Feedstock Industry" granted by Center of Excellence for Environmental and Hazardous Waste Management (EHWM) and Special Task Force for Activating Research (STAR) program of Chulalongkorn University. The authors are also grateful for support from the Research, Development and Engineering (RD&E) fund through The National Nanotechnology Center (NANOTEC), The National Science and Technology Development Agency (NSTDA), Thailand (Project No. P-11-00985) of Chulalongkorn University. This research was also supported by the Higher Education Research Promotion and National Research University Project of Thailand, Office of the Higher Education Commission (FW1017A). The authors wish to express their gratitude to Hitachi Scholarship Foundation for full support via the Hitachi Research Fellowship 2011. The technical support from Department of Environmental Engineering, Faculty of Engineering and the Center for Petroleum, Petrochemicals and Advanced Materials, Chulalongkorn University are also acknowledged.

References

[1] A. Rossner, S.A. Snyder, D.R.U. Knappe, Removal of emerging contaminants of concern by alternative adsorbents, Water Res. 43 (2009) 3787–3796.

[2] K.G. Karthikeyan, M.T. Meyer, Occurrence of antibiotics in wastewater treatment facilities in Wisconsin, USA, Sci. Total Environ. 361 (2006) 196–207.

[3] H.A. Duong, N.H. Pham, H.T. Nguyen, T.T. Hoang, H.V. Pham, V.C. Pham, M. Berg, W. Giger, A.C. Alder, Occurrence, fate and antibiotic resistance of fluoroquinolone antibacterials in hospital wastewaters in Hanoi, Vietnam, Chemosphere 72 (2008) 968–973.

[4] E. Zuccato, S. Castiglioni, R. Bagnati, M. Melis, R. Fanelli, Source, occurrence and fate of antibiotics in the Italian aquatic environment, J. Hazard. Mater. 179 (2010) 1042–1048.

[5] A.Y.-C. Lin, T.-H. Yu, C.-F. Lin, Pharmaceutical contamination in residential, industrial, and agricultural waste streams: Risk to aqueous environments in Taiwan, Chemosphere 74 (2008) 131–141.

[6] B. Halling-Sørensen, H.-C. Holten Lützhøft, H.R. Andersen, F. Ingerslev, Environmental risk assessment of antibiotics: Comparison of mecillinam, trimethoprim and ciprofloxacin, J. Antimicrob. Chemother. 46 (2000) 53–58.

[7] S.A.C. Carabineiro, T. Thavorn-amornsri, M.F.R. Pereira, P. Serp, J.L. Figueiredo, Comparison between activated carbon, carbon xerogel and carbon nanotubes for the adsorption of the antibiotic ciprofloxacin, Catal. Today 186 (2012) 29–39.

[8] S.A.C. Carabineiro, T. Thavorn-Amornsri, M.F.R. Pereira, J.L. Figueiredo, Adsorption of ciprofloxacin on surface-modified carbon materials, Water Res. 45 (2011) 4583–4591.

[9] P. Punyapalakul, T. Sitthisorn, Removal of ciprofloxacin and carbamazepine by adsorption on functionalized mesoporous silicates, World Acad. Sci. Eng. Technol. 69 (2010) 546–550.

[10] Z. Li, H. Hong, L. Liao, C.J. Ackley, L.A. Schulz, R.A. MacDonald, A.L. Mihelich, S.M. Emard, A mechanistic study of ciprofloxacin removal by kaolinite, Colloids Surf. B 88 (2011) 339–344.

[11] C.-J. Wang, Z. Li, W.-T. Jiang, J.-S. Jean, C.-C. Liu, Cation exchange interaction between antibiotic ciprofloxacin and montmorillonite, J. Hazard. Mater. 183 (2010) 309–314.

[12] C. Gu, K.G. Karthikeyan, Sorption of the antimicrobial ciprofloxacin to aluminum and iron hydrous oxides, Environ. Sci. Technol. 39 (2005) 9166–9173.

[13] J. Wang, S. Zheng, J. Liu, Z. Xu, Tannic acid adsorption on amino-functionalized magnetic mesoporous silica, Chem. Eng. J. 165 (2010) 10–16.

[14] J. Qu, G. Liu, Y. Wang, R. Hong, Preparation of Fe_3O_4–chitosan nanoparticles used for hyperthermia, Adv. Powder Technol. 21 (2010) 461–467.

[15] H. Tian, J. Li, Q. Shen, H. Wang, Z. Hao, L. Zou, Q. Hu, Using shell-tunable mesoporous Fe_3O_4@HMS and magnetic separation to remove DDT from aqueous media, J. Hazard. Mater. 171 (2009) 459–464.

[16] M.M. Smart, R.G. Rada, G.N. Donnermeyer, Determination of total nitrogen in sediments and plants using persulfate digestion. An evaluation and comparison with the Kjeldahl procedure, Water Res. 17 (1983) 1207–1211.

[17] Q. Wu, Z. Li, H. Hong, K. Yin, L. Tie, Adsorption and intercalation of ciprofloxacin on montmorillonite, Appl. Clay Sci. 50 (2010) 204–211.

[18] D. Avisar, Y. Lester, H. Mamane, PH induced polychromatic UV treatment for the removal of a mixture of SMX, OTC and CIP from water, J. Hazard. Mater. 175 (2010) 1068–1074.

[19] E.O. Augustine, Intraparticle diffusion process for lead(II) biosorption onto mansonia wood sawdust, Biores. Technol. 101 (2010) 5868–5876.

[20] P. Prarat, C. Ngamcharussrivichai, S. Khaodhiar, P. Punyapalakul, Adsorption characteristics of haloacetonitriles on functionalized silica-based porous materials in aqueous solution, J. Hazard. Mater. 192 (2011) 1210–1218.

[21] F.-C. Wu, R.-L. Tseng, R.-S. Juang, Initial behavior of intraparticle diffusion model used in the description of adsorption kinetics, Chem. Eng. J. 153 (2009) 1–8.

[22] G.F. Malash, M.I. El-Khaiary, Piecewise linear regression: A statistical method for the analysis of experimental adsorption data by the intraparticle-diffusion models, Chem. Eng. J. 163 (2010) 256–263.

[23] M.H. Kalavathy, T. Karthikeyan, S. Rajgopal, L.R. Miranda, Kinetic and isotherm studies of Cu(II) adsorption onto H_3PO_4-activated rubber wood sawdust, J. Colloid. Interf. Sci. 292 (2005) 354–362.

[24] I.A.W. Tan, A.L. Ahmad, B.H. Hameed, Adsorption isotherms, kinetics, thermodynamics and desorption studies of 2,4,6-trichlorophenol on oil palm empty fruit bunch-based activated carbon, J. Hazard. Mater. 164 (2009) 473–482.

[25] T.X. Bui, H. Choi, Influence of ionic strength, anions, cations, and natural organic matter on the adsorption of pharmaceuticals to silica, Chemosphere 80 (2010) 681–686.

[26] M. Brigante, G. Zanini, M. Avena, Effect of humic acids on the adsorption of paraquat by goethite, J. Hazard. Mater. 184 (2010) 241–247.

[27] J. Wang, C. Zheng, S. Ding, H. Ma, Y. Ji, Behaviors and mechanisms of tannic acid adsorption on an amino-functionalized magnetic nanoadsorbent, Desalination 273 (2011) 285–291.

[28] J. Lin, Y. Zhan, Z. Zhu, Y. Xing, Adsorption of tannic acid from aqueous solution onto surfactant-modified zeolite, J. Hazard. Mater. 193 (2011) 102–111.

[29] L. Pasqua, F. Testa, R. Aiello, S. Cundari, J.B. Nagy, Preparation of bifunctional hybrid mesoporous silica potentially useful for drug targeting, Micropor. Mesopor. Mater. 103 (2007) 166–173.

[30] D. Lombardo, L. Bonaccorsi, A. Longo, E. Proverbio, P. Calandra, Charge interaction of low generation dendrimers during zeolite formation, J. Non-Cryst. Solids. 357 (2011) 771–774.

[31] L. Pasqua, A. Procopio, M. Oliverio, R. Paonessa, R. Prete, M. Nardi, M. Casula, F. Testa, J. Nagy, Hybrid MCM-41 grafted by a general microwave-assisted procedure: A characterization study, J. Porous Mater. December (2012) 1–9.

[32] S. Mozia, M. Tomaszewska, Treatment of surface water using hydrid processes adsorption on PAC and ultrafiltration, Desalination 162 (2004) 23–31.

[33] H. Zhang, C.-H. Huang, Adsorption and oxidation of fluoroquinolone antibacterial agents and structurally related amines with goethite, Chemosphere 66 (2007) 1502–1512.

[34] C.-L. Zhang, G.-L. Qiao, F. Zhao, Y. Wang, Thermodynamic and kinetic parameters of ciprofloxacin adsorption onto modified coal fly ash from aqueous solution, J. Mol. Liq. 163 (2011) 53–56.

[35] C.-J. Wang, Z. Li, W.-T. Jiang, Adsorption of ciprofloxacin on 2:1 dioctahedral clay minerals, Appl. Clay Sci. 53 (2011) 723–728.

[36] C. Eichholz, M. Stolarski, V. Goertz, H. Nirschl, Magnetic field enhanced cake filtration of superparamagnetic PVAc-particles, Chem. Eng. Sci. 63 (2008) 3193–3200.